Direct observations of a micropit in an elastohydrodynamic contact

A.V. Olver*, L.K. Tiew, S. Medina, J.W. Choo

Tribology Section, Department of Mechanical Engineering, Imperial College London, Exhibition Road, London SW7 2AZ, UK

Abstract

A hard steel roller from a disc tester which had an isolated micropit and associated cracks on its surface was pressed against a glass plate and subjected to a range of lubricated, rolling–sliding conditions, with the objective of observing the effect on the distribution of film thickness in an EHL contact.

The results show a remarkable interaction between the micropit, the direction of sliding and the thickness of the elastohydrodynamic film. Fluid expulsion into the cavitated region can be observed as the micropit emerges from the contact.
© 2003 Elsevier B.V. All rights reserved.

Keywords: Micropit; EHL

1. Introduction

Rolling contact fatigue is a failure mode of contacting metallic surfaces which has been studied experimentally for many years. It is characterised by progressive cracking from an origin which is often situated on the extreme surface and may lead to the detachment of fragments of the affected component. It is usual to distinguish between *pitting* (or "macro-pitting" or spalling) in which the affected zone extends to roughly the depth of the dimensions of the area of contact and *micropitting* in which the affected depth is much less. Micropitting is particularly prevalent in ground steel surfaces and is usually attributed to the stress field associated with the roughness of the contacting surfaces.

For many years, it has been a matter of contoversy as to whether or not the propagation of cracks in rolling contact fatigue is influenced by, or even dependent upon, the presence of a fluid, such as a liquid lubricant. In Way's 1935 experiment [1], rolling fatigue only occurred when a liquid was present, perhaps because the liquid entered the crack and created an opening displacement, despite the predominantly compressive field of stresses. On the other hand, rolling fatigue cracks are common in railway tracks where liquid is often only present intermittently, in the form of rainwater [2].

Theoretical studies [3–5] have suggested that the fluid may act in one of two ways: either the fluid pressure acts directly on the crack mouth (fluid *pressurisation*) as a result of the high elastic pressure in the region of contact or, alternatively, fluid becomes entrapped in the crack and a region near the tip is pressurised by the motion of the area of contact across the surface (fluid *entrapment*). In recent years, it has become clear that the fluid entrapment mechanism provides an explanation of one significant feature of rolling fatigue.

In the early stages of growth, the cracks which give rise to pitting or micropitting are usually shallowly inclined to the surface as shown in Fig. 1. The direction of this inclination is determined only by the direction of the applied traction and is not affected by that of the motion of the contact itself. However, *propagation* of these initial cracks has been found to require that the area of contact moves across the cracked surface from the mouth of the crack toward its tip, a situation encountered on the "follower" of discs in tractive rolling – or in the dedendum of gears. Nakajima [6] confirmed this by actually reversing rolling and sliding directions after cracks had been initiated.

This situation, in which the motion of the contact across the surface strongly affects the rate of crack propagation and the development of subsequent damage, is easily explained by the fluid entrapment hypothesis: the motion of the contact toward the tip is required in order to raise the pressure near the tip and create a significant crack opening; motion in the opposite sense merely empties the crack of fluid. Analysis of this situation was carried out by Bower [3], by Murakami et al. [4] and by Matsuda et al. [5].

Experiments by Godet and co-workers [7] and subsequently by Xiaogang et al. [8], in which cracks extending to the side of a disc were observed during rolling contact,

---

* Corresponding author. Tel.: +44-20-7594-7066;
fax: +44-20-7823-8044.
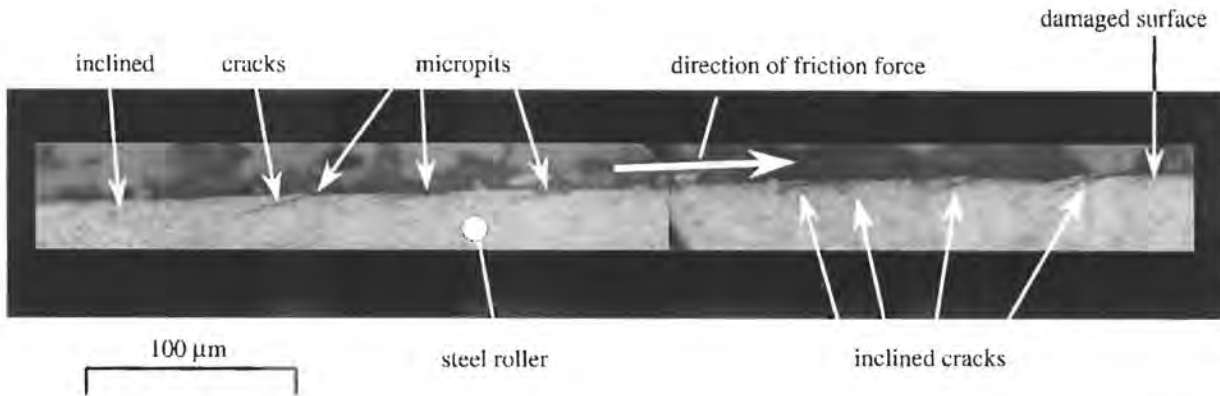*E-mail address:* a.v.olver@imperial.ac.uk (A.V. Olver).

Fig. 1. Cross section of typical micropitted surface in hard steel, showing relationship of crack inclination to direction of friction force.

tended to confirm that fluid did indeed flow into rolling fatigue cracks, but the cracks used were large and atypical in shape, so it has not been at all clear whether fluid entrapment could be a significant mechanism in the propagation of small defects such as micropits. There has also been remarkably little experimental work on the effect of fatigue cracks or pits on conditions in the contact—particularly important to the way in which the fluid might exert an influence upon the development and propagation of damage. However, in recent years, with the development and refinement of the optical technique, it has become possible to observe and measure the effect of passing many types of surface defects through lubricated contacts. Ridges, dents and bumps, in various orientations, both individually and in arrays have been studied [9–11].

Perhaps surprisingly, in view of its practical importance, little attention has been paid to the effect of an actual micropit. In this paper, we report on the effect of passing such a micropit, produced on a test roller in a contact fatigue ex-

periment, through an elastohydrodynamic contact. Rolling and sliding speeds were varied in magnitude and direction and interference images were obtained so that film shape and thickness could be determined.

2. Experiment

2.1. Fatigue testing

The rolling fatigue test was carried out using a three-contact disc machine which has been described in detail elsewhere [12]. The test was carried out at a Hertz pressure of 2.5 GPa and a slide–roll ratio ($\Delta v/\bar{v}$) of −30% (roller surface slower). (Here, Δv is the difference in speed and $\bar{v}$ is the mean speed of the surfaces with respect to the contact.)

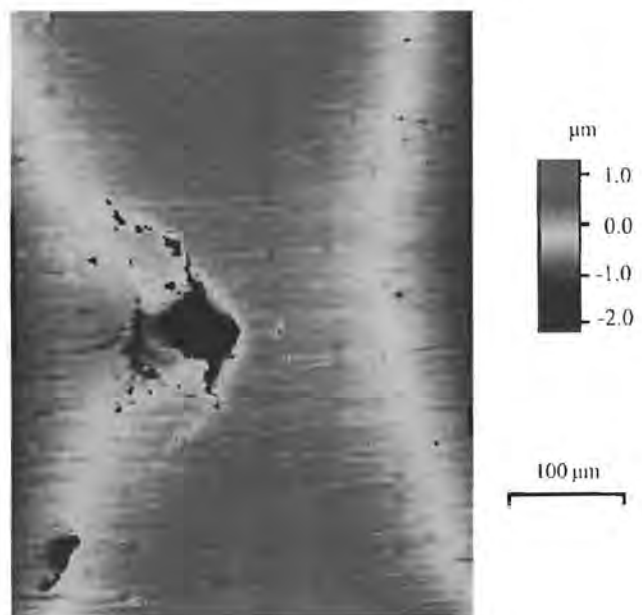Fig. 2. Optical micrograph of isolated micropit used for the present study.

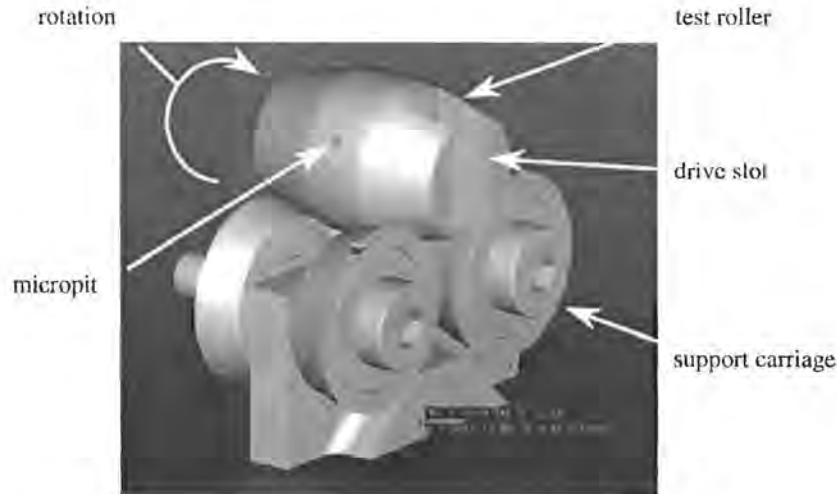Fig. 3. Surface topography of test micropit (Wyko).

Fig. 4. Specimen carriage used to support micropitted test roller in optical rig.

The specimen used was manufactured from vacuum induction melted, vacuum arc remelted AISI M50 steel (0.85% C, 0.3% Mn, 0.20% Si, 4.10% Cr, 4.25% Mo, 1.00% V) hardened from 1100 °C, triple tempered at 540 °C and deep frozen at −80 °C after the first temper, giving less than 3% retained austenite. The diameter of the roller was 18.593 mm with a crowning radius of 45.0 mm and its hardness was 61–64 HRc.

The roller was circumferentially ground and had a centre line average surface roughness of $R_a = 583.8$ nm, measured over a 1 mm length in the axial direction after the test.

The three counterface rollers were manufactured from BS970 722M24 (En 40b) steel (0.25% C, 3.2% Cr, 0.6% Mo) in condition T (0.2% proof stress = 850 MPa, minimum) ground and gas nitrided to 950 HV.

The lubricant used for the fatigue test was Castrol AN157, a poly-ol ester, formulated, transmission lubricant, having a viscosity of 10 cSt at 100 °C. The test was carried out at a sump temperature of 70 ± 2 °C for 9.24×10^5 cycles before being terminated automatically because of increased vibration which was found to be due to some surface micropitting. The contact inlet temperature was estimated to be 105 °C leading to an EHL film thickness of about 100 nm.

2.2. Details of features studied

In order to improve its optical properties, the test roller was lightly polished with 1200 grit silicon carbide paper followed by 3 μm and then 1 μm diamond slurry. This had the effect of reducing the surface roughness to $R_a = 327.6$ nm. A single micropit on the test roller was selected for further study and is shown in Fig. 2. The topography of the surface adjacent to the cracked region was measured using an interference microscope (Wyko) and is shown in Fig. 3. The micropit had a typical v-shape, about 100 μm in size and

had a surface crack leading away in the rolling direction for a distance of around 190 μm.

2.3. Film thickness testing

The test roller was then mounted on a special carriage (Fig. 4) enabling it to be pressed against the flat glass disc of an optical rig. The arrangement of the rig is shown in Fig. 5. All tests were carried out at a normal load of 20 N giving a Hertz pressure of 334 MPa and an elliptical area of contact of 566 μm × 202 μm. The direction of rotation was such that the narrow end of the pit entered the contact first as it had previously done in the disc machine. The bulk temperature was controlled to 40 ± 1 °C using electric heaters.

Optical interference images were obtained using the "Spacer Layer Imaging Method" (SLIM) which has been described earlier [11,13]. The lubricant used for this part of the work was a polyalphaolefin which had a viscosity of 0.1230 Pa s and a pressure viscosity coefficient of 24.7 GPa^{-1} at 40 °C.
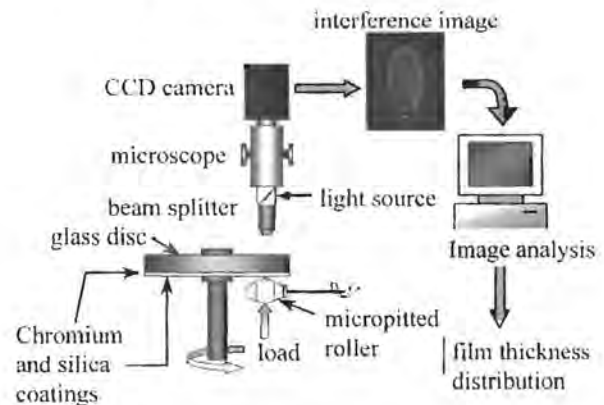

Fig. 5. Schematic of SLIM technique [13].

18.2 mm/s   27.7 mm/s   38.7 mm/s

51.6 mm/s   63.0 mm/s   76.4 mm/s

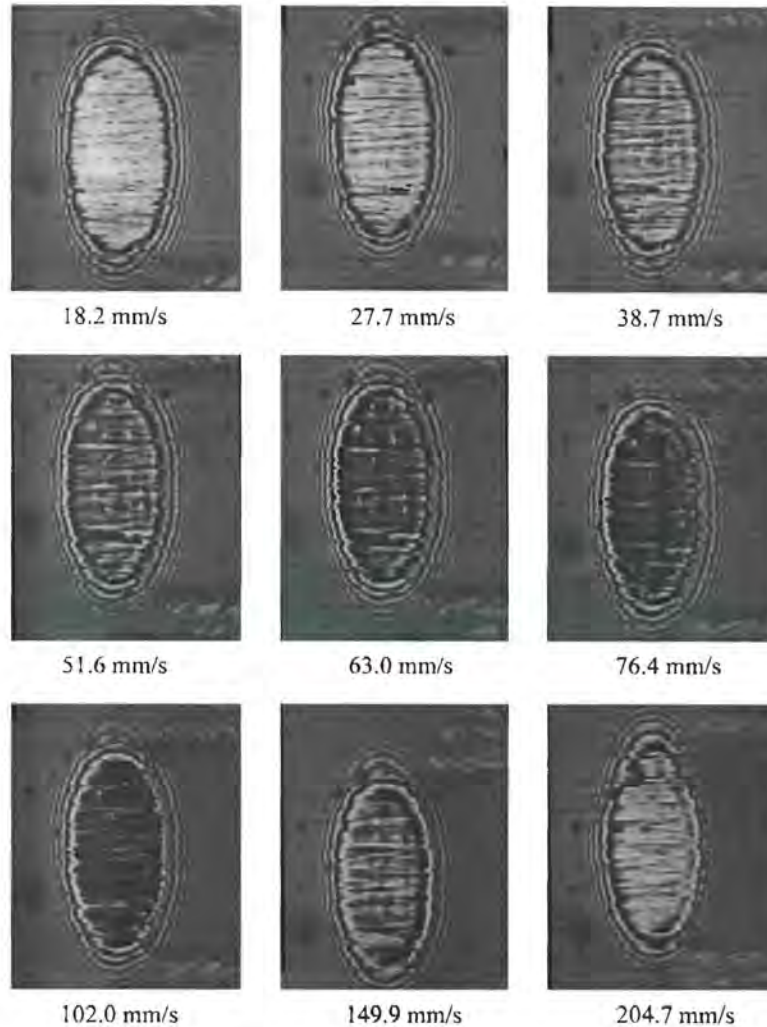102.0 mm/s   149.9 mm/s   204.7 mm/s

Fig. 6. Interference images of undamaged roller surface for a range of rolling speeds.

3. Results

3.1. Undamaged surface

Interference images for the undamaged surface are shown in Fig. 6 for a range of entrainment speeds in pure rolling. Fig. 7 shows the mean central film thickness as a function of rolling speed compared with that predicted by the Hamrock and Dowson equation [14]. The film was somewhat thinner than predicted, probably due to the effect of the longitudinal roughness. Changing the slide–roll ratio had a negligible effect on the thickness of the film formed by the undamaged roller.

3.2. Micropit in pure rolling

Fig. 8 shows a sequence of interference images of the micropit passing through the contact in pure rolling with (both) surfaces travelling at 100 mm/s. Two features associated with

the pit are apparent. Firstly, there is a region of much thinner film near the leading edge of the pit when near the centre part of the contact (Fig. 8c). (The central part of the pit appears dark on the interference image because there is no reflection
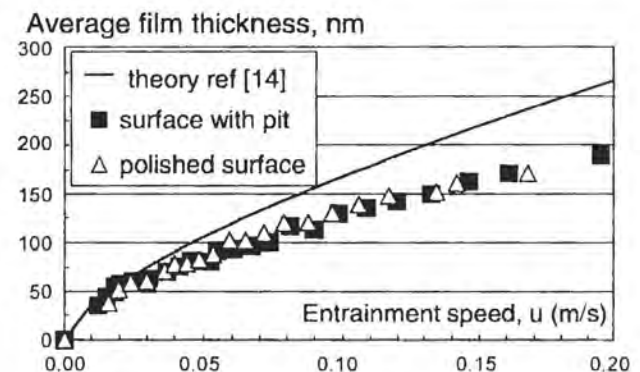

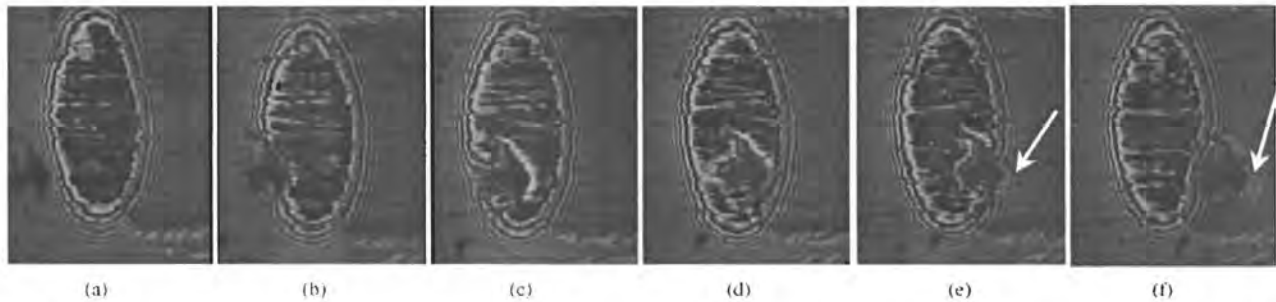Fig. 7. Comparison of mean film thickness with smooth surface prediction.

Fig. 8. Sequence of interference images showing micropit passing through contact in pure rolling. Entrainment speed = 100 mm/s. Arrows show fluid expelled into cavitated region.

from the underlying fracture surface.) Secondly, when the pit enters the cavitated region at the exit, fluid can be seen escaping (Fig. 8e and f). Away from the immediate vicinity of the pit, the film thickness was unaffected by its presence.

Varying the speed in pure rolling had little effect except to increase the thickness of the film remote from the micropit (Fig. 9). Again, the mean film away from the pit was similar to that of the undamaged surface.
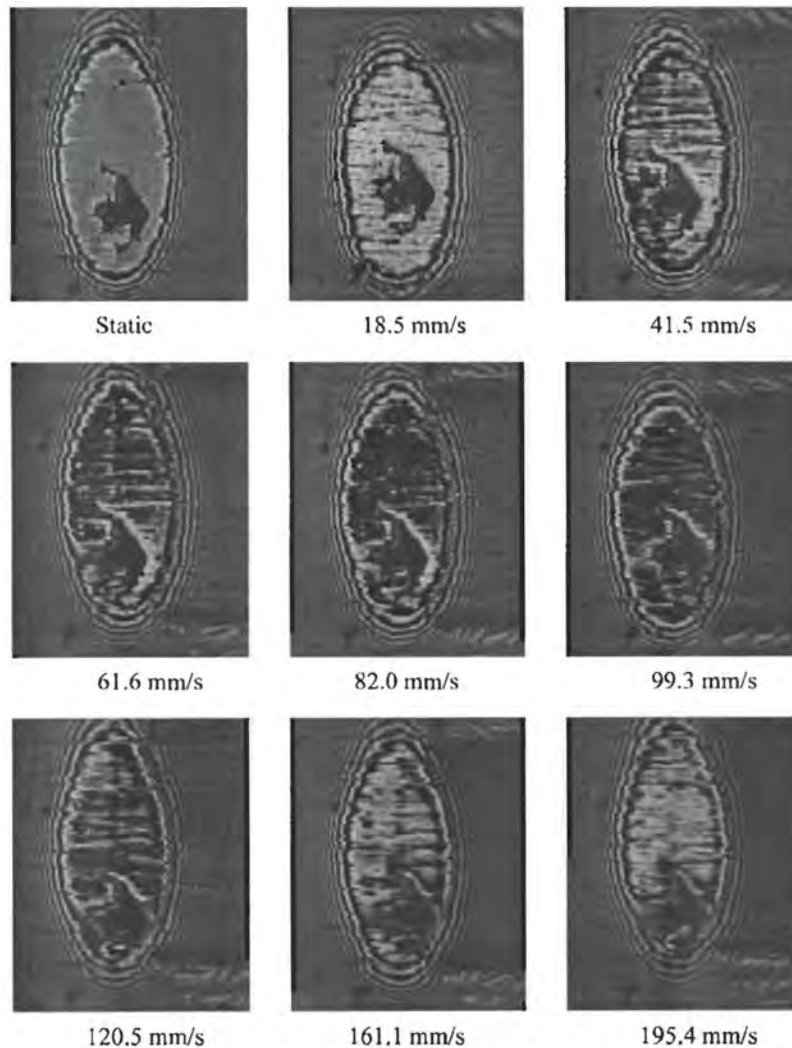

Fig. 9. Interference images showing micropit in contact at different rolling speeds.

Fig. 10. Interference images showing micropit passing through contact under conditions of positive slide–roll ratio.

film thickness, nm

- no micropit
- micropit present - Figure 11(a)
- micropit present - Figure 11(b)

50 µm

transverse position

Fig. 12. Film thickness along a transverse line just ahead of the micropit under conditions of negative slide–roll ratio.

3.3. Micropit in rolling–sliding

Next, the influence of sliding was investigated by altering the rotational speed of the disc and roller. A typical interference image for positive slide roll ratio (speed of disc surface = 49 mm/s, speed of micropitted roller surface = 149 mm/s) is shown in Fig. 10. It is similar to the pure rolling result except that the constriction near the leading edge of the pit appears somewhat less prominent.

The corresponding condition with *negative* slide roll ratio (speed of disc surface = 149 mm/s, speed of micropitted roller surface = 49 mm/s) is illustrated in Fig. 11, which shows a sequence of three images as the micropit passes through the contact. Here, the leading edge constriction is much more prominent and at one point extends about
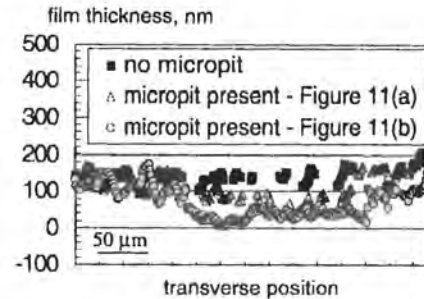
100 µm from the pit right across the contact to the exit (Fig. 11b).

In addition, the expulsion of fluid in the cavitated region is much more marked than in the corresponding pure rolling or positive slide roll ratio conditions (Fig. 11c).

The actual film thickness along a transverse line in the thinner region just ahead of the pit is shown in Fig. 12. (The location of this line is shown in Fig. 11b and c.) This shows a film thickness of around 40 nm and is less than 10 nm in some areas, compared to around 130 nm remote from the pit.

4. Discussion

The present feature differs considerably from any of those examined in earlier studies in two important respects. Firstly, it is much deeper. The pit region of the feature, although it could not be measured exactly, was probably of the order of 10 µm at the trailing edge. This is far deeper than any of the dents studied, for example, by Wedeven [9] and, of course, greatly exceeds the thickness of the film in the undamaged

expelled fluid

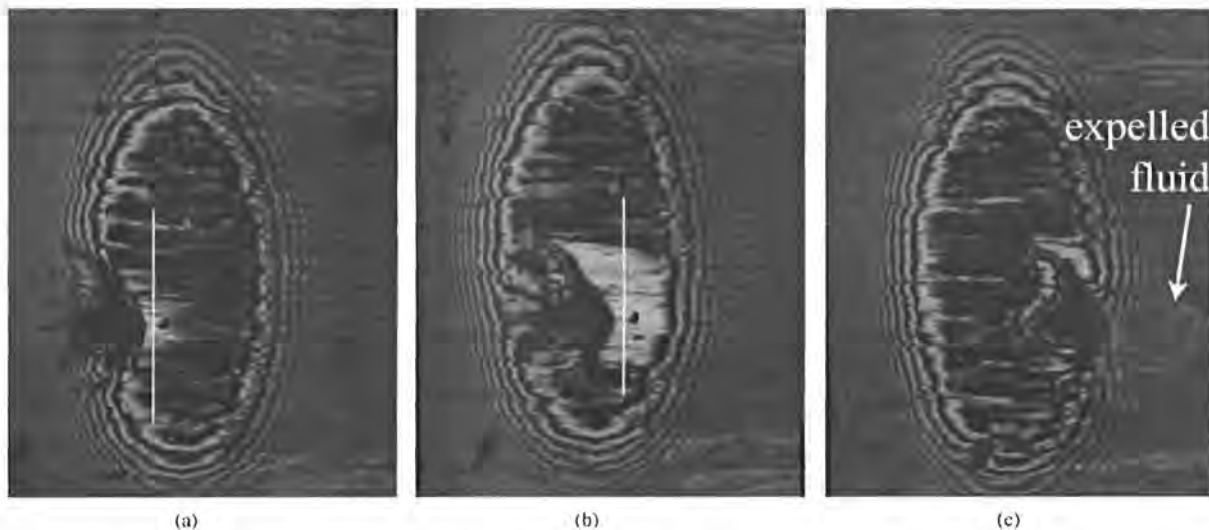(a)   (b)   (c)

Fig. 11. Sequence of interference images showing micropit passing through contact under conditions of negative slide–roll ratio. The vertical lines in (a) and (b) show the regions analysed in Fig. 12. Note large amount of fluid expelled into cavitated region in (c)—compare with Fig. 8e and f.

region. Secondly, the micropit has a large (200 μm) crack system attached to it which probably extends beyond the area of contact throughout most of its passage.

Both these differences suggest that the micropit may not behave simply as a surface irregularity in the manner of conventional micro-EHL theory, namely in accordance with coupled half-space elasticity and Reynolds' equation. Indeed it is apparent that under negative slide–roll ratios, the micropit does not behave at all like the shallow dents studied by Wedeven [9] and by Venner and Lubrecht [15]. Under negative sliding, Venner and Lubrecht showed that there was a "convected" perturbation leading to increased film thickness in precisely the region ahead of the feature where the present work shows a reduced film. (Wedeven seems to have had inconsistent results in sliding but recent results obtained by two of the present authors confirmed that Venner and Lubrecht's predictions are correct for a shallow dent in both positive and negative sliding). A likely reason for the difference between dents and the present micropit is the presence here of the additional path for fluid leakage provided by the crack.

The negative slide–roll ratio condition—that is: when the roller is the "follower", with a lower surface speed than that of the conterface—has long been known to be the most damaging condition for fatigue propagation [6]. The observations of a reduced or collapsed film ahead of the crack and of expulsion of an appreciable volume of fluid when the crack reaches the exit agree precisely with the fluid entrapment mechanism proposed by Bower and co-workers. The fact that neither rapid crack propagation nor—in this study—the reduced film thickness occur at positive slide–roll ratios may also be significant. Bower [3] attributed the former to the closure of the crack by frictional forces during its approach to the contact, preventing fluid ingress.

The present observations are strikingly similar to the much-studied phenomenon of starvation. In starvation, the oil supply is reduced, leading to the approach of the inlet meniscus (effectively a zero pressure boundary condition) to the contact and resulting in a local thinning of the film. If the starvation is transient, then the region of reduced film thickness "convects" through the contact at the mean rolling speed. In the present case, the pit may cause a (much) reduced pressure to be present, not because of restriction of the oil supply, as in starvation, but rather because of the leakage path provided by the crack system. Only in the negative slide–roll ratio condition can this reduced film region convect into the contact ahead of the defect—in positive sliding it would be swept into the deep part of the pit. To this, we may perhaps add Bower's conjecture that in positive sliding the crack would be closed and hence the leakage path obstructed.

Taken together, these considerations provide a compelling explanation for the present findings:

- In negative sliding (pit on slower surface), the crack system of the micropit is held open by frictional forces during its approach to the contact region. Since it contains a deep and extensive leakage path, the micropit reduces the local pressure to a low value as it passes into the inlet region. This causes a reduction in local film thickness, akin to transient starvation, which "convects" toward the exit at a speed greater than that of the pit, leading to the band of low film thickness seen in Fig. 11b and c.

- In contrast, positive sliding (pit on faster surface) leads to both the closure of the crack (reducing or removing the leakage path) and to the obscuring of any residual starvation by the defect itself.

- Finally, upon exit from the contact, fluid is expelled – a process assisted by the higher compressive loading caused by negative sliding (Figs. 8 and 11c).

5. Conclusions

1. The passage of an actual micropit, produced during a rolling fatigue test, through an elastohydrodynamic contact has been examined using the optical SLIM.

2. The results show a remarkable interaction between the micropit, the direction of sliding and the elastohydrodynamic film. Under negative slide–roll ratio, there is a large region of thinner film present. Fluid expulsion into the cavitated region can be observed as the micropit emerges from the contact.

3. The results are consistent with the conjecture of fluid entrapment and subsequent expulsion advanced by Bower and others and are also strongly reminiscent of transient starvation. Fluid flow or leakage into the pit and its associated crack system provides a plausible explanation.

References

[1] S. Way, Pitting due to rolling contact, Trans Am. Soc. Mech. Eng., J. Appl. Mech. 57 (1935) A49–A58.

[2] W.R. Tyfour, J.H. Beynon, A. Kapoor, Deterioration of rolling contact fatigue life of pearlitic rail steel due to dry–wet rolling–sliding line contact, Wear 197 (1996) 255–265.

[3] A.F. Bower, The influence of crack face friction and trapped fluid on surface initiated rolling contact fatigue cracks, Trans. Am. Soc. Mech. Eng., J. Tribol. 110 (1988) 704–711.

[4] Y. Murakami, M. Kaneta, H. Yatsuzuka, Analysis of surface crack propagation in lubricated rolling contact, ASLE Trans. 28 (1985) 209–216.

[5] K. Matsuda, A.V. Olver, E. Ioannides, Propagation of rolling contact fatigue cracks by the fluid entrapment mechanism, in: Presentation to the World Tribology Congress, London, 1997 (abstract only published).

[6] A. Nakajima, Effect of asperity interacting frequency on surface durability, in: International Symposium on Gearing and Power Transmissions, paper b26, Tokyo, 1981.

[7] B. Michau, D. Berthe, M. Godet, Observations of oil pressure effects in surface crack development, Tribol. Int. 7 (1974) 119–122.

[8] L. Xiaogang, C. Qing, E. Shao, Initiation and propagation of case crushing cracks in rolling contact fatigue, Wear 122 (1988) 33–43.

[9] L.D. Wedeven, Influence of debris dent on EHD lubrication, ASLE Trans. 21 (1) (1978) 41–52.

[10] M. Kaneta, A. Cameron, Effects of asperities in elastohydrodynamic lubrication, J. Lubrication Technol. 102 (1980) 374–379.

[11] J.W. Choo, A.V. Olver, H.A. Spikes, Influence of surface roughness features on mixed film lubrication, Lubrication Sci. 15 (3) (2003) 219–232.

[12] A.V. Olver, H.A. Spikes, P.B. Macpherson, Wear in rolling contacts, Wear 112 (1986) 121–144.

[13] P.M. Cann, H.A. Spikes, The development of a spacer layer imaging method (SLIM) for mapping elastohydrodynamic contacts, Tribol. Trans. 39 (4) (1996) 915–921.

[14] B.J. Hamrock, D. Dowson, Ball Bearing Lubrication, Wiley, New York, 1981.

[15] C.H. Venner, A.A. Lubrecht, Transient analysis of surface features in an EHL line contact in the case of sliding, Trans. Am. Soc. Mech. Eng., J. Tribol. 116 (1994) 186–193.